NMR IN BIOMEDICINE
NMR Biomed. 2005;**18**:383–389
Published online 13 July 2005 in Wiley InterScience (www.interscience.wiley.com). DOI:10.1002/nbm.970

A model of lysosomal metabolism of dextran coated superparamagnetic iron oxide (SPIO) nanoparticles: implications for cellular magnetic resonance imaging†

Ali S. Arbab,* Lindsey B. Wilson, Parwana Ashari, Elaine K. Jordan, Bobbi K. Lewis and Joseph A. Frank

Experimental Neuroimaging Section, Laboratory of Diagnostic Radiology Research, National Institutes of Health, Bethesda, Maryland, USA

Received 16 December 2004; Revised 10 March 2005 & 20 April 2005; Accepted 4 May 2005

ABSTRACT: Ferumoxides, dextran-coated superparamagnetic iron oxide (SPIO) particles, form ferumoxide–transfection agent (FE–TA) complexes that are internalized into endosomes/lysosomes and have been used to label cells for *in vivo* MRI tracking and localization studies. A better understanding of the physical state of the FE–TA complexes during endocytosis could improve their use. The purpose of this study was to measure the rate of the degradation of iron particles under varying physiological conditions. FE–TA complexes were incubated in seven different buffers containing different chelates with different pH. Reducible iron concentrations, T_2 relaxation rates and gradient echo (GRE) magnetic resonance images (MRI) were obtained from each condition immediately after incubation and at 6, 24, 48, 72 and 96 h and days 7, 14 and 21. The dynamics of FE–TA in the endosome/lysomes within the cells were visualized with electron microscopy. Sodium citrate buffer at pH 4.5 rapidly dissolved FE–TA complexes. However, FE–TA complexes were less soluble in the same buffer at pH 5.5. Similarly, FE–TA complexes were not readily soluble in any of the other buffers with or without chelates, regardless of pH. Electron microscopic images showed degraded FE–TA in some intracellular endosome/lysosomes between days 3 and 5. In the cellular environment, some of the FE–TA-containing endosomes were found to fuse with lysosomes, causing rapid dissociation at low pH and exposing the iron core to chelates that resulted in soluble Fe(III) within the lysosomes. The studies presented represent a first step in identifying the important cellular environmental parameters affecting the integrity of FE–TA complexes. Published in 2005 by John Wiley & Sons, Ltd.

KEYWORDS: Ferumoxides; SPIO; Endosome/lysosome; Poly-L-lysine; Labeled cells

INTRODUCTION

Ferumoxide is a clinically approved dextran-coated superparamagnetic iron oxide (SPIO) nanoparticle MRI contrast agent, used for delineating tumors in the liver.[1,2] Kupffer cells of the liver, part of the reticuloendothelial system (RES), sequester ferumoxides and metabolize SPIO nanoparticles.[3] However, the metabolic pathway for the degradation of the dextran-coated iron oxide nanoparticles by Kupffer cells has not been elucidated. Following phagocytosis, the iron oxide nanoparticles are transferred from early to deep endosomes in the cell where they may fuse with lysosomes and the environment increases in acidity from neutral to a pH of 4.5–5. Monocrystalline iron oxides have been shown to accumulate at the perinuclear vesicles, which may represent terminal lysosomes, in which degradation of the nanoparticles occurs *in vitro* and these lysosomes have an increase in enzymatic activity following iron loading of the cells.[4–6]

Cellular uptake of iron (Fe) (iron that binds to transferrin) occurs through receptor-mediated endocytosis of the Fe(III)–transferrin complex. Iron dissociates from transferrin in a low pH environment found in endosomes. Iron is ultimately transferred from the endosome into the cytoplasm, where it can enter into the intracellular labile iron pool, form low-molecular-weight iron complexes or high-molecular-weight intermediates. The iron may be used for metabolic function of the cell, stored in ferritin or ultimately contribute to heme synthesis in red blood cells (RBC).[7] The transport of iron from the endosome into the cytosol involves binding of the iron to various low-molecular-weight compounds, such as citrate and isocitrate.[8,9] There has been speculation that these dicarboxylic acid chelates may form complexes with the free iron.

A method has recently been developed to label different types of cells with ferumoxides complexed with poly-L-lysine (PLL). It has been assumed that the incorporation of the ferumoxide–PLL complexes into cells is by fluid-phase endocytosis, although the exact

**Correspondence to:* A. S. Arbab, Radiology Research, Henry Ford Health System, 1 Ford Place, Box 82, Detroit, MI 48202, USA.
E-mail: Saali@rad.hfh.edu

Abbreviations used: BPS, bathophenanthroline disulfonic acid; FE–TA, ferumoxides-transfection agent; GRE, gradient echo; MSC, mesenchymal stem cells; PLL, poly-L-lysine; RBC, red blood cells; RES, reticuloendothelial system; SA, sodium acetate; SC, sodium citrate; SPIO, superparamagnetic iron oxide.

mechanism of the cellular uptake of the complex has not been determined. A recent study demonstrated that uptake of ferumoxides nanoparticles is accomplished by scavenger receptor SR-A mediated endocytosis in macrophages.[10] Preliminary data has shown that the iron particles remain transiently in endosomes/lysosomes of rapidly dividing cells and, following five to eight cell divisions, iron could not be detected in the cells on Prussian blue stain or by T_2 relaxometry.[11–13] However, the physical state of the ferumoxides in the lysosomes and how the cell metabolizes these particles have not been elucidated. The insignificant transiently increased production of ROS in FE–PLL-labeled cells suggests that complexes dissolve in the endosomal/lysosomal environment and Fe is being released into the cytoplasm.[13]

Skotland *et al.*[14] have utilized an *in vitro* lysosomal model using different pH and chelates to determine the status of iron oxide nanoparticles with an oxidized starch coating. In the current study, we have extended this work using an *in vitro* model of the intracellular lysosomal environment with different buffering systems (with or without chelates) and varying degrees of pH to determine the rate of the physical degradation of the ferumoxides nanoparticles in relation to varying physiological conditions. FE–PLL-labeled cells were also analyzed by electron microscopy and by T_2 relaxometry to determine the status of the complexes inside the endosomes/lysosomes and the changes in signal intensity on MRI that result from the SPIO nanoparticles dissolving in labeled cells.

MATERIALS AND METHODS

Buffers

Seven incubation buffers were prepared: I = RPMI-1640 (R) at pH 7; II = RPMI-1640 at pH 5.5;III = RPMI-1640 at pH 4.5; IV = 20 mM sodium citrate (SC) in RPMI-1640 at pH 5.5; V = 20 mM SC in RPMI-1640 at pH 4.5; VI = 20 mM sodium acetate (SA) in RPMI-1640 at pH 5.5; and VII = 20 mM SA in RPMI-1640 at pH 4.5. Concentrated HCl was added to adjust the pH of solutions II and III, citric acid was added to adjust the pH of solutions IV and V, and glacial acetic acid was used to adjust the pH of solutions VI and VII. All buffers were filtered through a 0.22 μm (3M Milipore, Billerica, MA, USA) filter to make them sterile. RPMI-1640 is a cell culture medium and was obtained from commercial vendor (Biosource International, Camarillo, CA, USA). All other chemicals were obtained from Sigma (Sigma, St Louis, MO, USA).

Ferumoxides–poly-L-lysine complex

Ferumoxides at a concentration of 50 μg/ml and PLL at a concentration of 1.5 μg/ml were added to RPMI-1640 medium without any serum and mixed with a rotator for 60 min. A volume of the solution containing FE–PLL complexes was then added to equal volume of buffers and kept at 37 °C in a 5% CO_2 incubator in a total of seven silicon-coated flasks, one for each buffer. The final concentrations of ferumoxides and PLL were 25 and 0.75 μg/ml. After repeated mechanical disruption with a pipette to disperse the large complexes, a specific volume of each solution from each flask was collected at 0, 6, 24, 48, 72 and 96 h as well as at days 7, 14, and 21 for nuclear magnetic resonance (NMR) relaxation rates, magnetic resonance imaging (MRI) and measurement of Fe(III) in the mixtures.

Measurement of free Fe(III) in the buffers containing FE–PLL complexes

The core of ferumoxides consists of magnetite (γFe_2O_3) with dextran absorbed onto the surface of the nanoparticle.[15] If the appropriate pH and/or chelates are present in the buffered solutions, the iron core should dissolve and free Fe(III) will be released into the solution. The presence of free Fe(III) would indicate the effect of different buffer systems on the FE–PLL complex. Bathophenanthroline disulfonic acid (BPS; 4,7-diphenyl-1, 10-phenanthroline disulfonic acid) was obtained from Sigma (St Louis, MO, USA) and a stock solution of 4.95 mM was prepared to measure the reduced iron in the experimental preparations. BPS forms color with reduced iron [Fe(II)], that can be measured using a UV spectrometer at 535 nm absorbance wavelength. Free Fe(III) can be reduced to Fe(II) by ascorbate. All absorbance measurements were performed on a UV spectrometer (Shimadzu, Columbia, MD, USA) using a 1 ml disposable cuvette. Incubation mixtures I–VII were analyzed at 0, 6, 24, 48, 72 and 96 h, and 7, 14 and 21 days. Before analysis at each time point, a fresh 100 mM ascorbate solution was prepared and kept on ice. Incubation mixtures were diluted 9:1 by combining 100 μl of each sample and 900 μl of the corresponding buffer solution in a disposable cuvette. To each cuvette containing the 1 ml diluted sample, 40 μl of BPS were added. After 90 s, the absorbance of each sample was read at 535 nm and then 20 μl of ascorbate solution were added to each cuvette followed by measurement of the absorbance at 535 nm after 8 min. To get the final absorbance values of each sample at each time point, the positive differences of the post-BPS readings and the post-BPS-ascorbate readings were used.

The concentration of free Fe(III) in the samples at each time point was calculated by normalizing the data to a standard curve. Free Fe(III) content was expressed in mmol/l. A standard curve was prepared using five solutions of Fe(III) citrate at 0.0, 0.005, 0.01, 0.05 and 0.1 mmol/l. One milliliter of each solution was added to a cuvette and mixed with 40 μl BPS. The absorbance was read at 535 nm after 90 s. A 20 μl aliquot of freshly

prepared ascorbate solution (100 mmol) was added to each sample, and the absorbance was read at 535 nm after 8 min. Final absorbance values for each solution were determined as the positive difference between the absorbance after BPS addition and the absorbance after both BPS and absorbance values. A standard curve was prepared by plotting the final absorbance value vs solution concentration for each of the five solutions.

Magnetic resonance relaxation parameters and effects of different forms of irons

Magnetic resonance images are based on the signal from hydrogen nuclei contained in hydrogen-rich compounds in the body. Based on the hydrogen content and hydrogen nuclei relaxation time (T_1, T_2 and T_2^*), MR image contrast is achieved. T_1 relaxation requires a dipole–dipole interaction between adjacent fluctuating electron and/or proton.[16–18] One of the parameters that regulate dipole–dipole interaction is the distance between two fluctuating fields.[18] The most effective enhanced T_1 relaxation requires a contrast agent [such as paramagnetic Gd(III), Fe(III), Mn(III), etc.] interacting with hydrogen nuclei when the contrast agent comes into close proximity with water molecules.[16,18] Enhanced T_1 relaxation (shortening of T_1 relaxation time) leads to higher (increased) signal intensity on T_1-weighted MRI. Free Fe(III) proton relaxation enhancement would result in high signal intensity on T_1-weighted MRI. T_2 (also T_2^*) relaxation (transverse or spin–spin relaxation) depends on the magnetic field inhomogeneities.[16–18] Superparamagnetic or high concentrations of paramagnetic substances shorten the transverse relaxation time.[18] These agents can create magnetic field inhomogeneities that are broader than the molecules, and diffusion of water molecules through these gradients promotes dephasing of the associated proton transverse magnetization.[16–18] The amount of T_2 dephasing induced by a superparamagnetic agent depends on the following: (a) contrast agent; (b) the pulse sequences; (c) echo time (*TE*); and (d) the path followed by the water molecules.[16,18–21] Superparamagnetic iron oxide nanoparticles are a crystalline form of iron that creates magnetic field inhomogeneity and dephasing of transverse relaxtion, causing susceptibility effects. Gradient-echo pulse sequences are more sensitive to changes in magnetic susceptibility. Enhancement of transverse relaxation causes lower (decrease) signal intensity on MRI.

NMR relaxometry

In order to determine the spin–spin relaxation times (T_2) of the mixtures containing iron nanoparticles, a sample volume was analyzed using a custom-built NMR relaxometer. T_2 relaxation times are dependent on the integrity of SPIO nanoparticles. Once SPIO nanoparticles are dissolved and the iron is release into the mixtures, there would be dramatic change and prolongation of T_2 relaxation times. The analysis was performed immediately after preparation of the mixtures and after the mixtures were incubated for 6, 24, 48, 72 and 96 h and 7, 14 and 21 days. For each of the seven incubation mixtures, 0.5 ml of the mixture was mixed with 0.5 ml 16% gelatin in NMR tubes, mixed thoroughly, and rapidly frozen on ice to set the gelatin. The solid samples were stored at 4 °C. NMR T_2 relaxation times were obtained at 23 °C and measurements were performed at 1.0 T (i.e. 42 MHz). T_2 relaxation times were obtained using a Carr–Purcell–Meiboom–Gill (CPMG) pulse sequence with 500 echoes and an inter-echo time (tau) of 1 ms. For this study, the T_2 relaxation times are expressed as the relaxation rate ($1/T_2$) in seconds^{-1}.

MR imaging

MR imaging of the mixtures in gelatin was performed at 1.5 T (Signa II, GE, Milwaukee, WI, USA) using a 5-inch surface coil. MR imaging was performed using a multislice gradient echo (GRE) sequence [*TR* (repetition time) = 300 ms, *TE* = 20 ms and a flip angle = 20°]. Images were obtained with a matrix size of 256 × 160, NEX (number of excitations) = 2, slice thickness = 2 mm and a field of view (FOV) = 10 × 10 cm. Signal intensities (SI) from the images of the tubes were determined from a circular 35 mm^2 region of interest (ROI). Owing to susceptibility artifacts of the iron oxide nanoparticles on GRE images, there would be low signal intensity on MRI as long as SPIO nanoparticles remain intact. However, if free iron was present following the breaking down of nanoparticles, the susceptibility effects of the nanoparticles should decrease and an increase in the signal intensity would be detected on GRE images. In addition, since Fe(III) is paramagnetic, the T_1 relaxation properties of the water protons would shorten and also contribute to the increase in signal intensity in the images since GRE images has some degree of T_1 weighting contributing to the signal intensities observed in the image.

Intracellular lysosomal degradation of FE–PLL complexes

To determine the effect of the intracellular lysosomal environment on the FE–PLL complexes, mesenchymal stem cells (MSCs) were cultured and labeled with FE–PLL complexes (25:0.75 μg/ml) overnight as previously described,[12,13] washed twice with sterile PBS and replaced with fresh complete culture medium without FE–PLL complexes. In short, MSCs were incubated at 80–100% confluent in the culture flasks overnight with medium containing FE–PLL complexes. Labeled cells were collected at different time points from 1 h to 5 days.

The collected cells were fixed with 3% gluteraldehyde, washed three times with 0.1 M sodium cacodylate buffer, re-suspended in 10% warm agarose in an Eppendorf microtube and immediately centrifuged (at 6000–10 000 rpm) to collect the cells at the bottom. Once the agarose gel hardened, the tip of the Eppendorf tube was clipped off and the agar removed out the top of the tube. The area with the cells was cut out (usually at the tip of the agar) and then re-suspended in 0.1 M (normal solution) cacodylate buffer until ready for processing. The cell–agar pellet was placed in 2% osmium tetraoxide in 0.1Na cacodylate buffer for 2 h. The osmium was removed and cell–agar pellet was washed three times with 0.1 M cacodylate buffer. Cells were then fixed in 1% uranyl acetate in 0.1 M acetate buffer overnight and then fixed in a Lynx automated processor (EMS, Hatfield, PA, USA) with alcohol dehydration, propylene oxide dehydration and through epon infiltration. After hardening in an epon mold at 60 °C overnight, the cell–agar pellets were sectioned at 50–70 nm and mounted on copper grids. The grids were stained in uranyl acetate or with uranyl acetate and lead citrate. The specimens were imaged with a transmission electron microscope (Jeol 200 CX, Peabody, MA, USA).

RESULTS

Release of free iron

Release of free Fe(III) from the FE–PLL complexes was both pH and chelate dependent (Fig. 1) and was largest when the complex was incubated in the buffer system containing SC at pH 4.5. Measurable free Fe(III) was detected as soon as the complexes were added to the buffer and the concentration of the iron in medium reached a maximum level by 7 days. Sodium citrate buffer at pH 5.5 also contained measurable free Fe(III) in the solution by 48 h, but the iron concentration was lower than that in SC in RPMI at pH 4.5. For all other buffers, including SA, at various pH levels there was no detectable increase in measurable free Fe(III) until day 21 (Fig. 1).

T_2 relaxation rates and MRI

T_2 relaxation rates ($1/T_2$ in s^{-1}) of the gelatin tubes containing the mixtures of different pHs and chelates with FE–PLL complex, and MRI at different time points along with the corresponding signal intensities of ROI measurement are shown in Fig. 2. The decrease in the T_2 relaxation rates for the FE–PLL complexes when mixed with SC in RPMI at pH 4.5 occurred early and decreased to a greater extent as compared with the other combinations of buffers over a range of pH and chelates. The MRI clearly demonstrates an increase in signal intensity of solutions containing the SPIO nanoparticle complexed to the PLL when mixed with SC buffer at pH 4.5 starting at 96 h. The increase in signal intensity corresponds to the detected increase in free paramagnetic Fe(III). Starting at day 14 there was a slight decrease in T_2 relaxation rates observed with all other buffers, except in buffered solutions containing SA. The MRI showed a slight increase in signal intensity with SC buffer at pH 5.5 starting at day 14 compared with the other buffers (except sodium citrate at

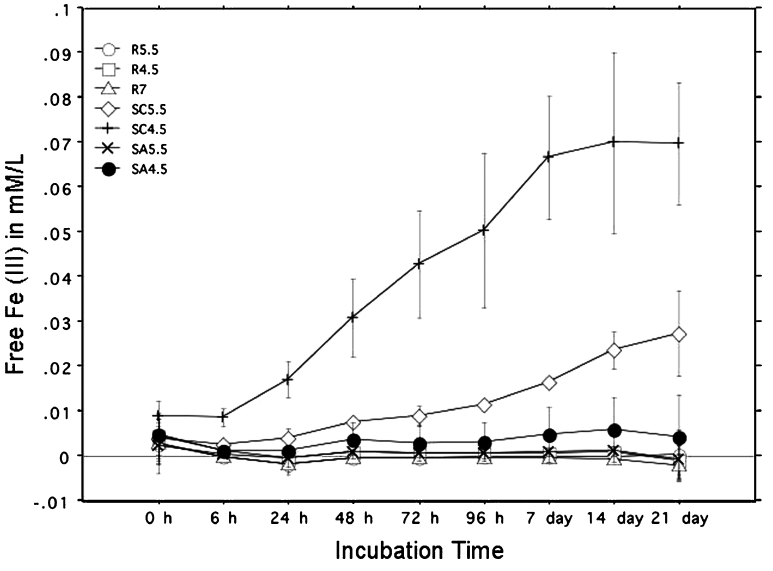

Figure 1. Reducible free iron in the buffers at different time points is shown. Note the release of iron only in sodium citrate buffers. R = RPMI-1640 medium; SC = sodium citrate; SA = sodium acetate. The number (5.5, 4.5 and 7) indicates the pH of the solutions. The *x*-axis indicates the time when the buffers with complexes were analyzed

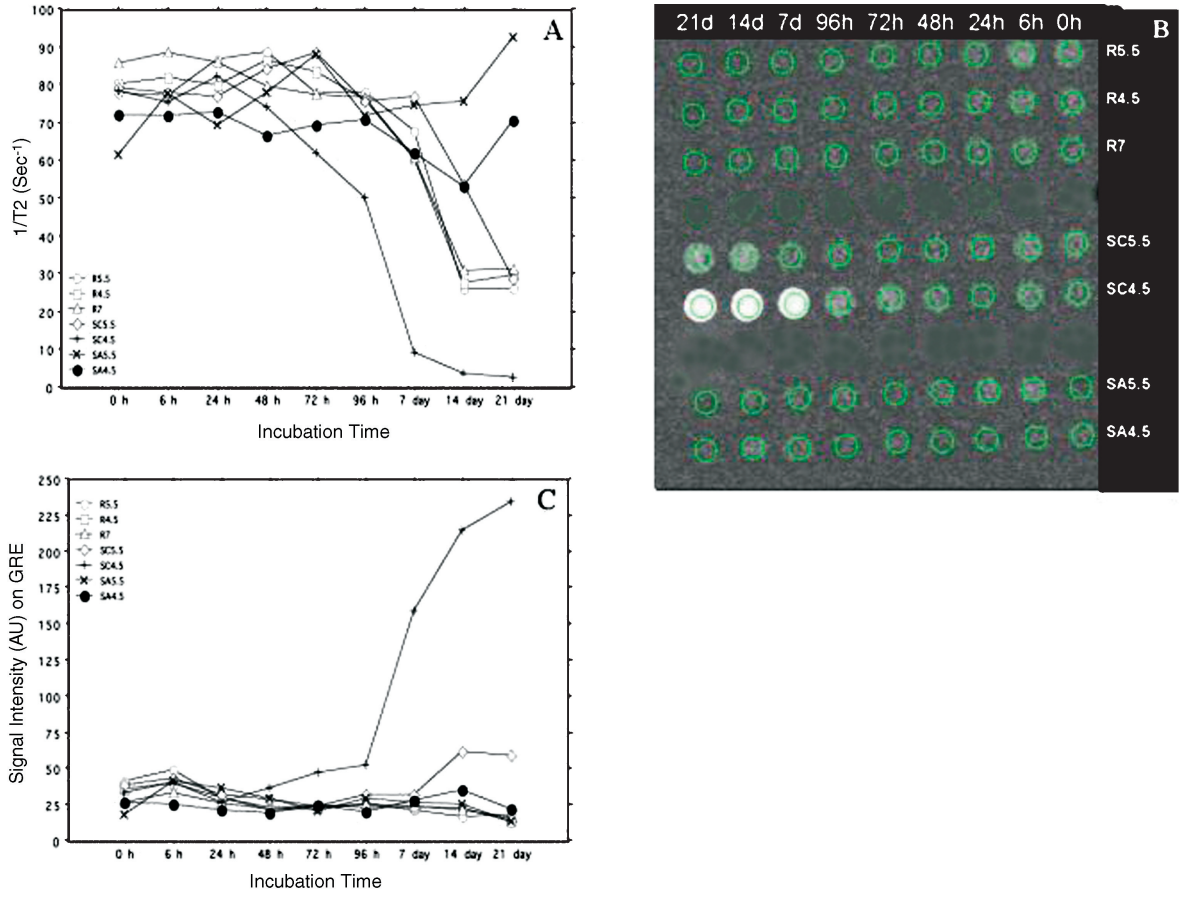

Figure 2. T_2 relaxation rates (A), GRE images (B) and corresponding signal intensity (C) of the buffers containing FE–PLL complexes in gelatin. Buffers containing FE–PLL complexes were collected at different times and quickly frozen in gelatin. Note the loss of T_2 relaxation rates and the susceptibility effect of ferumoxides in buffers containing sodium citrate. Both MRI (B) and corresponding signal intensity (C) indicate loss of the particulate form of iron. The *x*-axis indicates the time when the buffers with complexes were collected. R = RPMI-1640 medium; SC = sodium citrate; SA = sodium acetate. The number (5.5, 4.5 and 7) indicates the pH of the solutions

pH 4.5), suggestive of a slow rate of dissolving of the nanoparticles.

Lysosomal degradation of FE–PLL in cells

To determine the effect of endosomal/lysosomal environment on the intracellular FE–PLL complexes, cells were labeled and collected at different time points and subjected to electron microscopic examination. By 1 h post-incubation of cells with FE–PLL, the complexes were attached along the cell membrane and intracellular uptake was noted by 3 h (Fig. 3). FE–PLL complexes usually form multiple branching processes. Unless the complexes disintegrate or dissolve, it is expected that a similar configuration would remain inside the cellular endosomes/lysosomes. Branching complexes were seen within endosomes as early as 3 h [Fig 3(B)] and they became compact over time [Fig. 3(C)]. Limited numbers of endosomes containing FE–PLL complexes were seen fusing with clear vacuoles by 72 h [Fig. 3(D)]. The branching configuration of FE–PLL complexes was less visible on EM (electron microscope) by day 5 and in some endosomes/lysosomes dissolved particles (arrows) were observed by day 5 [Fig. 3(E)].

DISCUSSION

The main findings of the current study are that we were able to demonstrate that FE–PLL complexes dissolved at low pH (pH 4.5) in a model of lysosomal environment containing SC chelates. Metabolism of ferumoxides occurs in experimental systems within 30 days;[7] however, it is unclear what the physical state is of the iron oxide nanoparticles in the endosomes or the microenvironment required to dissolve these nanoparticles, making the free iron available for metabolic pathways. Iron homeostasis in the circulation has been well delineated and is robust. An increase in free iron concentration in the serum is guarded by increased transferrin that subsequently transports the free iron to cells.[22–25] Cellular iron homeostasis

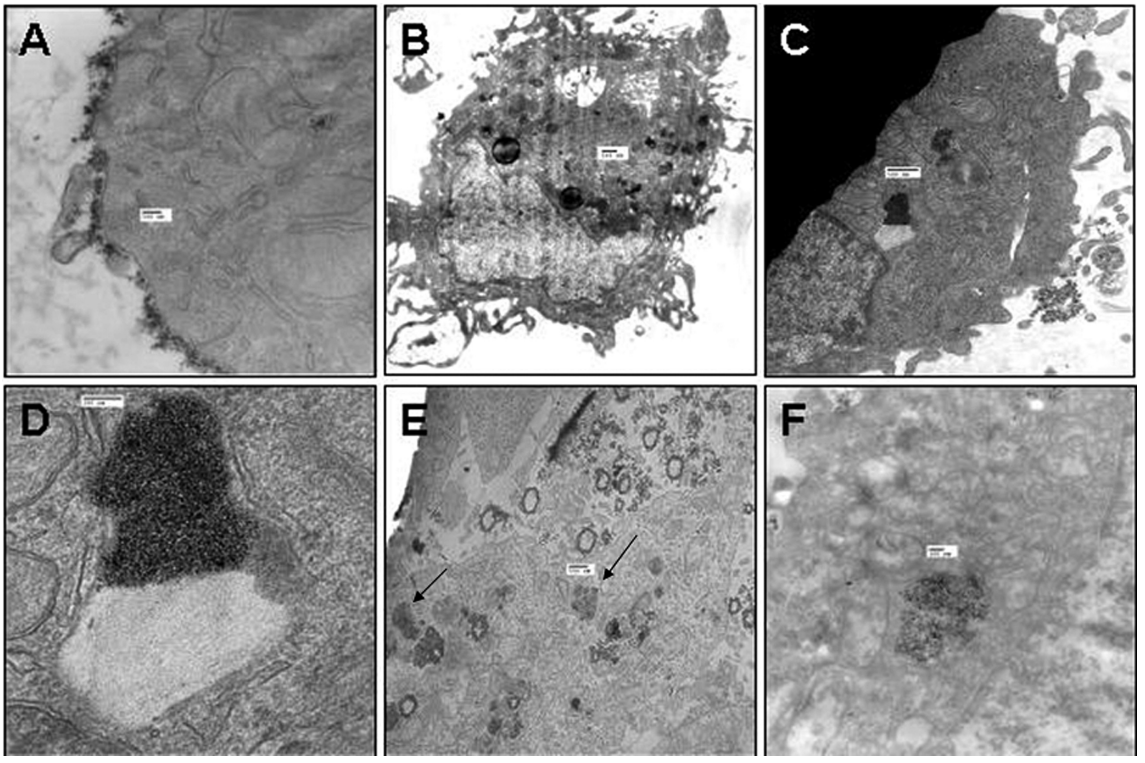

Figure 3. Electron microscopic images of mesenchymal stem cells from 1 to 120 h (5 days) after labeling with FE–PLL complexes. Note the attachment of the complexes along the cell membrane at 1 h (A), endosomal incorporation by 3 h (B), endosomes packed with the complexes (C) and fusion of endosome containing the complexes with lysosomes (D) and degradation (arrows) of the complexes at day 5 (E) and close-up view of endosome/lysosome causing degradation of the complexes (F). Scale bars on A, D and F are 100 nm. The scale bar on B, C and E is 500 nm

results from an interaction of both cellular transferrin receptors and cytoplasmic ferritin to maintain the cytoplasmic iron concentration below the threshold level to prevent the formation of free radicals and reactive oxygen species.[26–28] Increases in free radicals due to reduced cellular iron (FeII) result in increased production of radical oxygen species (ROS) that may initiate lipid peroxidation and ultimately damage DNA.[22,29]

We have reported that cells labeled with FE–PLL complexes show an insignificant transient rise in the production of ROS in the initial few days following labeling.[13] We hypothetized that the low pH environment and presence of citrate or similar metallic chelates within the endosome/lysosome might dissolve the FE–PLL complexes, resulting in release of free Fe(III) into the cytoplasm through the divalent cationic transport. Although exact mechanisms of dissolving iron nanoparticles by SC were not investigated in this study, there have been reports showing that citrates have a greater affinity for ferric iron (Fe[III]) than ferrous iron (Fe[II]) and facilitate absorption of iron.[30,31] Dicarboxylic acids, such as citrate, form a more stable complex with transferrin and ferric iron.[32] In the current study, it can be concluded that both the presence of chelates (i.e. citrate) that have a greater affinity for Fe(III) vs Fe(II) and an acidic lysosomal environment would dissolve FE–PLL complexes by 96 h. The degradation of the ferumoxide nanoparticles to free Fe(III) in the buffers at appropriate pH was demonstrated by the decrease in T_2 relaxation rates, an increase in signal intensity on gradient echo imaging with T_2 and T_2^* weighting. Since labeled cells containing intact iron complexes behave as a large superparamagnetic contrast agent, causing dephasing and T_2^* shortening in MRI tracking of labeled cells in tissues for relatively long periods of time, the dominant relaxation mechanisms appear to be due to T_2 and T_2^* shortening and not an enhancement of T_1 relaxation.[33] Electron microscopy also demonstrated that the FE–PLL changed their configuration over time when in the intracellular endosomal/lysosomal environment (Fig. 3). However, the changes in the appearance of the FE–PLL were not observed in all of the endosomes. This finding suggests that there may be mechanisms or signals within cells not dissolving all the iron complexes in endosomes simultaneously, thereby preventing the formation of ROS and cellular toxicity. These findings would also be supported by the transient insignificant increase in ROS production in labeled cells in our previous study.[13] We did not attempt to quantify the number of endosomes/lysosomes on EM that dissolved the FE–PLL complexes, because there is no established method to quantify the data from small sections of cells on EM images.

In conclusion, by utilizing the *in vitro* lysosomal environment, we have demonstrated the conditions necessary to alter the physical state of FE–PLL nanoparticle complexes inside cells. FE–PLL complexes enter cells by endocytosis and usually remain in the endosomes or may circulate back out into the extracellular space in rapidly dividing cells. Some of the endosomes may fuse with lysosomes containing low-pH medium and appropriate/specific chelates, which dissolve the dextran-coated iron oxide nanoparticles. The majority of the endosomes containing FE–PLL appear not to fuse with lysosomes and therefore the ferumoxides remain as nanoparticles compartmentalized within endosomes and are observed on T_2 and T_2^*-weighted imaging as hypointense regions on cellular MRI.

REFERENCES

1. Ferrucci JT, Stark DD. Iron oxide-enhanced MR imaging of the liver and spleen: review of the first 5 years. *AJR Am. J. Roentgenol.* 1990; **155**: 943–950.
2. Pouliquen D, Le Jeune JJ, Perdrisot R, Ermias A, Jallet P. Iron oxide nanoparticles for use as an MRI contrast agent: pharmacokinetics and metabolism. *Magn. Reson. Imag.* 1991; **9**: 275–283.
3. Weissleder R, Stark DD, Engelstad BL, Becon BR, Compton CC, White DL, Jacobs P, Lewis J. Superparamagnetic iron oxide: pharmacokinetics and toxicity. *AJR Am. J. Roentgenol.* 1989; **152**: 167–173.
4. Schulze E, Ferrucci JT, Poss K, lapointe L, Bogdanova A, Weissleder R. Cellular uptake and trafficking of a prototypical magnetic iron oxide label *in vitro*. *Invest. Radiol.* 1995; **30**: 604–610.
5. Link G, Pinson A, Hershko C. Iron loading of cultured cardiac myocytes modifies sarcolemmal structure and increases lysosomal fragility. *J. Lab. Clin. Med.* 1993; **121**: 127–134.
6. Yu Z, Persson HL, Eaton JW, Brunk UT. Intralysosomal iron: a major determinant of oxidant-induced cell death. *Free Radic. Biol. Med.* 2003; **34**: 1243–1252.
7. Richardson DR, Ponka P. The molecular mechanisms of the metabolism and transport of iron in normal and neoplastic cells. *Biochim. Biophys. Acta* 1997; **1331**: 1–40.
8. Conrad ME, Umbreit JN, Moore EG. Iron absorption and transport. *Am. J. Med. Sci.* 1999; **318**: 213–229.
9. Moos T, Morgan EH. The metabolism of neuronal iron and its pathogenic role in neurological disease: review. *Ann. NY Acad. Sci.* 2004; **1012**: 14–26.
10. Raynal I, Prigent P, Peyramaure S, Najid A, Rebuzzi C, Corot C. Macrophage endocytosis of superparamagnetic iron oxide nanoparticles: mechanisms and comparison of ferumoxides and ferumoxtran-10. *Invest. Radiol*. 2004; **39**: 56–63.
11. Frank JA, Miller BR, Arbab AS, Zywicke HA, Jordan EK, Lewis BK, Bryant LH Jr, Bulte JW. Clinically applicable labeling of mammalian and stem cells by combining superparamagnetic iron oxides and transfection agents. *Radiology* 2003; **228**: 480–487.
12. Arbab AS, Bashaw LA, Miller BR, Jordan EK, Bulte JW, Frank JA. Intracytoplasmic tagging of cells with ferumoxides and transfection agent for cellular magnetic resonance imaging after cell transplantation: methods and techniques. *Transplantation* 2003; **76**: 1123–1130.
13. Arbab AS, Bashaw LA, Miller BR, Jordan EK, Lewis BK, Kalish H, Frank JA. Characterization of biophysical and metabolic properties of cells labeled with superparamagnetic iron oxide nanoparticles and transfection agent for cellular MR imaging. *Radiology* 2003; **229**: 838–846.
14. Skotland T, Sontum PC, Oulie I. *In vitro* stability analyses as a model for metabolism of ferromagnetic particles (ClariscanTM), a contrast agent for magnetic resonance imaging. *J. Pharm. Biomed. Anal.* 2002; **28**: 323–329.
15. Jung CW. Surface properties of superparamagnetic iron oxide MR contrast agents: ferumoxides. ferumoxtran, ferumoxsil. *Magn. Reson. Imag.* 1995; **13**: 675–691.
16. Hendrick RE, Haacke EM. Basic physics of MR contrast agents and maximization of image contrast. *J. MRI* 1993; **3**: 137–148.
17. Nitz WR, Reimer P. Contrast mechanisms in MR imaging. *Eur. Radiol.* 1999; **9**: 1032–1046.
18. Wood ML, Hardy PA. Proton relaxation enhancement. *J. MRI* 1998; **3**: 149–156.
19. Hardy PA, Henkelman RM. On the transverse relaxation rate enhancement induced by diffusion of spins through inhomogenesous fields. *Magn. Reson. Med.* 1991; **17**: 348–356.
20. Josephson L, Lewis J, Jacobs P, Hahn PF, Stark DD. The effects of iron oxides on proton relaxivity. *Magn. Reson. Imag.* 1988; **6**: 647–653.
21. Majumdar S, Zoghbi SS, Gore JC. The influence of pulse sequence on the relaxation effects of superparamagnetic iron oxide contrast agents. *Magn. Reson. Med.* 1989; **10**: 289–301.
22. Emerit J, Beaumont C, Trivin F. Iron metabolism, free radicals, and oxidative injury. *Biomed. Pharmacother.* 2001; **55**: 333–339.
23. Arosio P, Levi S. Iron and cellular redox status. *Free Rad. Biol. Med.* 2002; **33**: 457–463.
24. Aisen P, Wessling-Resnick M, Leibold EA. Iron metabolism. *Curr. Opin. Chem. Biol.* 1999; **3**: 200–206.
25. Trinder D, Fox C, Vautier G, Olynyk JK. Molecular pathogenesis of iron overload. *Gut* 2002; **51**: 290–295.
26. Crichton RR, Wilmet S, Legssyer R, Ward RJ. Molecular and cellular mechanisms of iron homeostasis and toxicity in mammalian cells. *J. Inorg. Biochem.* 2002; **91**: 9–18.
27. Crinhton RR, Ward RJ. An overview of iron metabolism: molecular and cellular criteria for selection of iron chelators. *Curr. Med. Chem.* 2003; **10**: 997–1004.
28. Garner B, Roberg K, Brunk UT. Endogenous ferritin protects cells with iron-laden lysosomes against oxidative stress. *Free Rad. Res.* 1998; **29**: 103–114.
29. Gutteridge JMC, Rowley DA, Halliwell B. Superoxide-dependent formation of hydroxyl radical and lipid peroxidation in the presence of iron salt: detection of catalytic iron and antioxidant activity in extracellular fluids. *Biochem. J.* 1982; **206**: 605–609.
30. Moutafchiev DA, Sirakov LM, Ovcharroff VA. Effect of ascorbic acid, sodium citrate, sodium bicarbonate, and their combination effect on the binding of $59Fe^{2+}$ and $59Fe^{3+}$ to plasma membrane of lactating mouse mammary gland. *J. Inorg. Biochem.* 1990; **40**: 323–329.
31. Schmid A, Jakob E, Berg A, Russmann T, Konig D, Irmer M, Keul J. Effect of physical exercise and vitamin C on absorption of ferric sodium citrate. *Med. Sci. Sports Exerc.* 1996; **28**: 1470–1473.
32. Schlabach MR, Bates GW. The synergistic binding of anions and Fe^{3+} by transferrin. Implications for the interlocking sites hypothesis. *J. Biol. Chem.* 1975; **250**: 2183–2188.
33. Arbab AS, Jordan EK, Wilson LB, Yocum GT, Lewis BK, Frank JA. *In vivo* trafficking and targeted delivery of magnetically labeled stem cells. *Hum. Gene Ther.* 2004; **15**: 351–360.